

## **Numerical modelling of ice pressure effects on the ice resistance during station keeping in broken ice**

Marnix van den Berg<sup>1</sup>, Raed Lubbad<sup>1</sup>, Sveinung Løset<sup>1</sup>

<sup>1</sup>Department of Civil and Environmental Engineering, NTNU, NO-7491 Trondheim

### **ABSTRACT**

Loads from broken ice can be the governing design condition for structures and/or operations assisted by ice management. The ice resistance in broken ice is influenced by environmental factors such as the ice concentration, the ice floe size distribution, the ice drift speed, the ice thickness, and the ice mechanical properties. Full-scale observations show that in-plane pressure is another important parameter governing the ice resistance characteristics. This study investigates the effects of ice pressure on the interaction mechanisms and ice resistance occurring during a station keeping operation of a drill ship in drifting managed ice. For a single geometrical representation of a broken ice field, a range of boundary and ice pressure conditions are numerically simulated. The effects of ice pressure on the ice resistance are studied for two ship hull geometries. One ship has a bow with a high normal angle at the waterline (72°), while the other ship has a much lower normal angle at the bow (38°). The simulation results show that in-plane ice pressure has a much stronger effect on the ice resistance of the ship with the higher normal angle at the bow. The stronger effect of ice pressure is attributed to a more dominant role of in-plane ice clearing as a load releasing mechanism at steep normal angles, while out-of-plane clearing of ice is more dominant at lower normal angles. In-plane clearing resistance is more strongly influenced by ice pressure than out-of-plane clearing resistance.

**KEY WORDS:** Broken ice; pressured ice; Station-keeping

### **INTRODUCTION**

This study examines the influence of confinement conditions and ice pressure in broken (managed) ice fields. It is a follow-up study, following from a series of numerical simulations performed in the concept selection stage of a scientific drilling campaign ("ArcOP," 2022). The simulations performed in the preparation for ArcOP studied the station-keeping performance of four ships in several managed ice conditions. Among other parameters, the influence of different boundary or far-field conditions was simulated. The simulation results revealed that a boundary of rigid confining walls resulted in significantly higher ice resistance than a far-field condition of large ice floes (replacing the confining walls), in which the ice floes could move freely. It was observed that the boundary or far-field influence was related to the build-up of in-plane pressure in the broken ice field in the case of rigid boundaries, caused by the movement of the ship relative to broken ice field. In addition, the

simulation results showed that the influence of boundary conditions was significantly larger for some ships than for others. This observation led to the following questions:

- How, and through what mechanisms, is the effect of boundary conditions and ice pressure on the ice resistance in broken ice related to the ship hull shape?
- Can in-plane pressure caused by ship propagation in a confined domain of broken (managed) ice be seen as equivalent to mild ‘external’ pressure caused by wind and/or current?

Possible answers to these questions are sought in this study by performing discrete numerical simulations.

Pressured ice conditions occur most often in the vicinity of shorelines in combination with onshore winds or currents, but may also occur in the open ocean. Pressured ice in the open ocean can occur due to convergent wind or current fields (Turnbull et al., 2019). The ice pressure forecast visualized in Lemieux et al. (2020) shows many areas of (simulated) pressured ice in the open ocean.

In-plane pressure in ice fields has a strong influence on the ice loads experienced by ships or structures. It may influence the ice loads through the following mechanisms:

- By leading to the formation of pressure ridges (Kubat et al., 2012).
- By increasing the frictional resistance along the parallel mid-body of a ship (Li et al., 2019).
- By preventing or restricting the clearance of ice around the structure or ship hull.

As will be shown in this study, the prevention or restriction of ice clearance around the ship hull is found to be relevant in high-concentration (~90%) broken or managed ice conditions under mild (0 – 6 kN/m) external pressure.

The simulations described in this study cover three different far-field and boundary condition cases with no initial in-plane ice pressure and seven different in-plane ice pressure conditions. Each environmental condition is simulated for two ships: the Dina Polaris and the Vidar Viking. The simulations are performed with the Simulator for Arctic Marine Structures (SAMS). A summary of the main simulator characteristics is given in Section 3. The simulation results are compared by the simulated mean ice resistance and the observed interaction phenomena. The main results are described in Section 4. Section 5 discusses the validity bounds and limitations of the simulations performed in this study. Finally, the main conclusions are summarised in Section 6.

The results reveal that the ship hull shape strongly influences the effect of ice pressure on the ice resistance. Furthermore, the simulations show that the increase in ice resistance in the simulated broken ice conditions mainly results from the restriction of in-plane clearance of ice, and resistance from ice friction at the parallel mid-body is relatively unimportant.

## **SIMULATED CONDITIONS**

The simulations discussed in this study cover three different boundary or far-field conditions, seven different ice pressures, and 2 ship hull geometries. For each ship, three simulations are performed with no initial in-plane pressure. In these simulations, 3 different boundary or far-

field conditions are simulated. In addition, seven different ice pressure conditions are simulated for each ship, leading to a total of 20 different simulations (10 for each ship).

Table 1 lists the main geometrical properties of the two simulated ships: the Dina Polaris and the Vidar Viking. Both have similar dimensions, with the Dina Polaris being slightly larger than the Vidar Viking. However, the two ships have very different bow shapes. The Dina Polaris has a bulbous bow and a steep normal angle at the waterline, while the Vidar Viking has a V-shaped bow and a much lower average normal angle.

Table 1. Main geometrical properties of the simulated ships.

Ship	Stem angle (at waterline) [°]	Waterline entrance angle [°]	Normal angle bow (at waterline) [°]	Beam [m]	Length at waterline [m]
Dina Polaris	60	35	72	21	97
Vidar Viking	24	35	38	18	75

Table 2 lists the floe size and thickness distribution of the simulated managed ice field. The ice management operation itself is not modelled in this study. The floe size and thickness distribution represents an approximate upper limit for the expected operating conditions of the ArcOP drilling campaign. Random broken ice fields were numerically generated following this floe size and thickness distribution. The floe shapes of the numerically created broken ice field were obtained from a digitized top-view photo of actual broken ice, as shown in van den Berg et al. (2019b). The floe polygons obtained from the top view photo were scaled to match the floe size distribution listed in Table 2.

Table 2. Floe size and thickness distribution of the simulated managed ice field.

Diameter [m]	Thickness [m]	Percentage [%] (of total ice area)
1.5 - 5	1.0	25
5 - 10	1.5	25
10 - 20	1.5	20
10 - 20	2.0	20
20 - 25	2.5	8
20 - 25	3.5	2

Table 3 lists the main ice mechanical properties and the environmental parameters used in all simulations reported in this study. The ice mechanical properties are representative for first-year sea ice. All simulations are performed with initially static ice and the ships moving with a constant speed in the  $x$ -direction (as indicated in Figure 3 and Figure 4). Ship dynamics and the thrust properties of both ships are not considered in this study.

Table 3. Mechanical and environmental properties used in each simulation.

Ice concentration [%]	90.0	Ice-ship interaction velocity [knots]	1.0
Ice fracture toughness [kPa√m]	150.0	Fr. coeff. ice-ice [-]	0.25
Ice crushing pressure [MPa]	2.0	Fr. coeff. ice-structure [-]	0.1
Ice flexural strength [MPa]	0.5	Water density [kg/m <sup>3</sup> ]	1025
Ice tensile strength [MPa]	0.5	Ice density [kg/m <sup>3</sup> ]	910

In the following sections, we first describe the simulation setup of the simulations with no initial in plane pressure. Then, we describe the simulations setup of the pressured ice conditions.

### **Boundary conditions in simulations with no initial in-plane pressure**

For the same managed ice field, different boundary conditions were simulated in order to assess the influence of the assumed boundary conditions on the ice resistance. The simulated boundary conditions include two far-field ice conditions and a domain confined for 90% by rigid walls. The far-field ice conditions represent 90% concentration broken ice fields with different formation histories. Figure 1 shows satellite images of the two different far-field conditions that the numerical simulations aim to capture (the images are for illustration purposes only, and are not used directly to create the numerical ice fields).

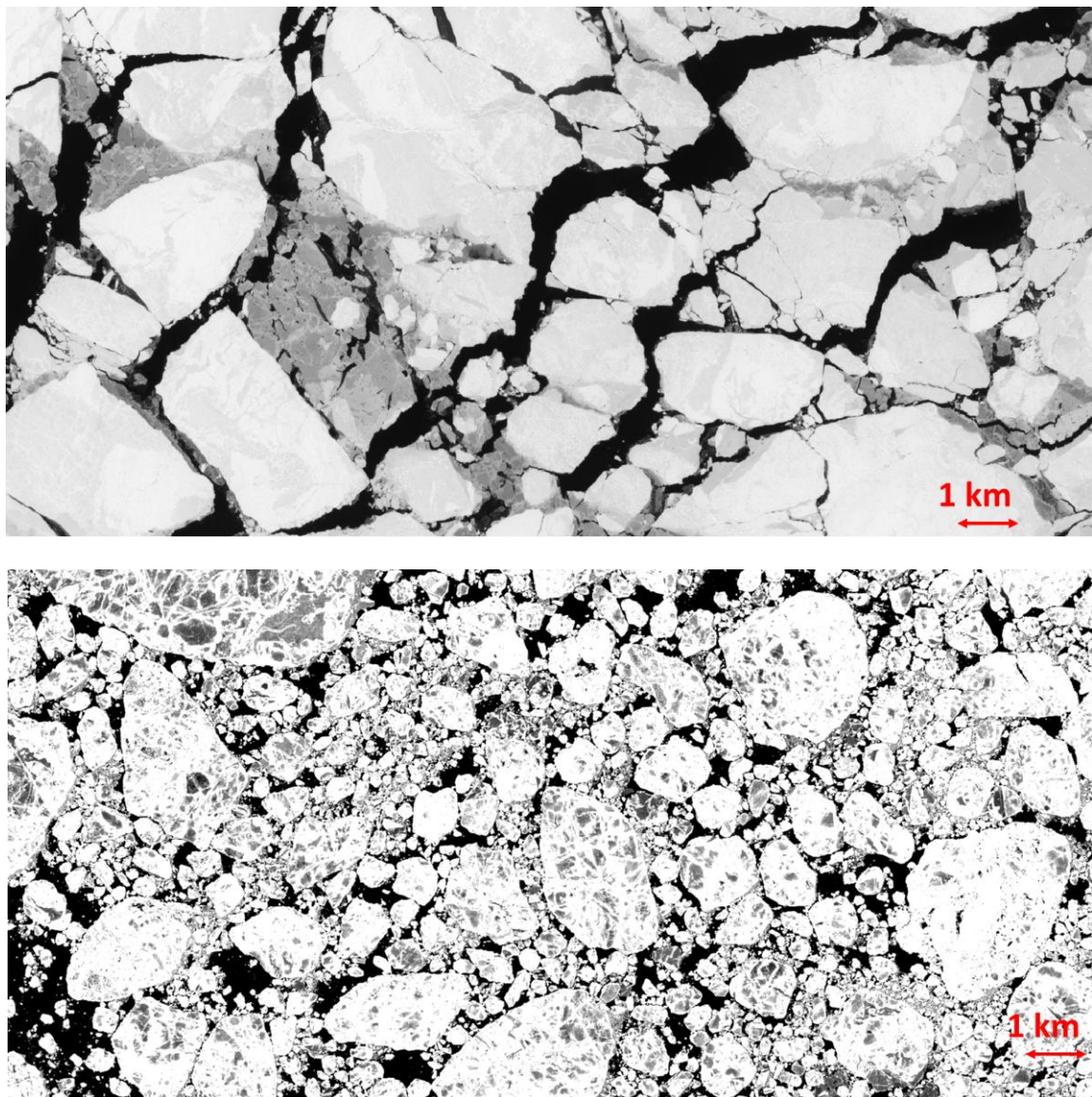


Figure 1. Two ice fields with a similar ice concentration but with different formation histories and environmental forcing (Copernicus Sentinel 2 satellite data, 2016-2019).

The top figure shows an ice field that is recently broken under the influence of wind and current shear. The ice floes are more angular in shape, and there are long continuous leads between the ice floes. This condition may occur under divergent environmental forcing. The lower figure shows an ice field with a similar concentration, but with a different formation history. The more rounded floe shapes indicate that this broken ice field has experienced significant ice-ice interactions. Importantly, the floes appear to form a continuous contact network, potentially enabling the occurrence of in-plane ice pressure.

Figure 2 shows the numerical representation of the simulated far-field conditions. The left figure represents a recently formed broken ice field with an ice concentration of 90%. The floes are angular, and there are long continuous leads between the floes. As a result, the displacement of far-field floes is initially only resisted by their inertia and drag. The right figure represents an older broken ice field with a concentration of 90%; the floes are more rounded, and the ice floes form a continuous contact network. The continuous contact network limits the extent to which the far field floes can move. In-plane pressure may result from propagation of the ship in the managed ice.

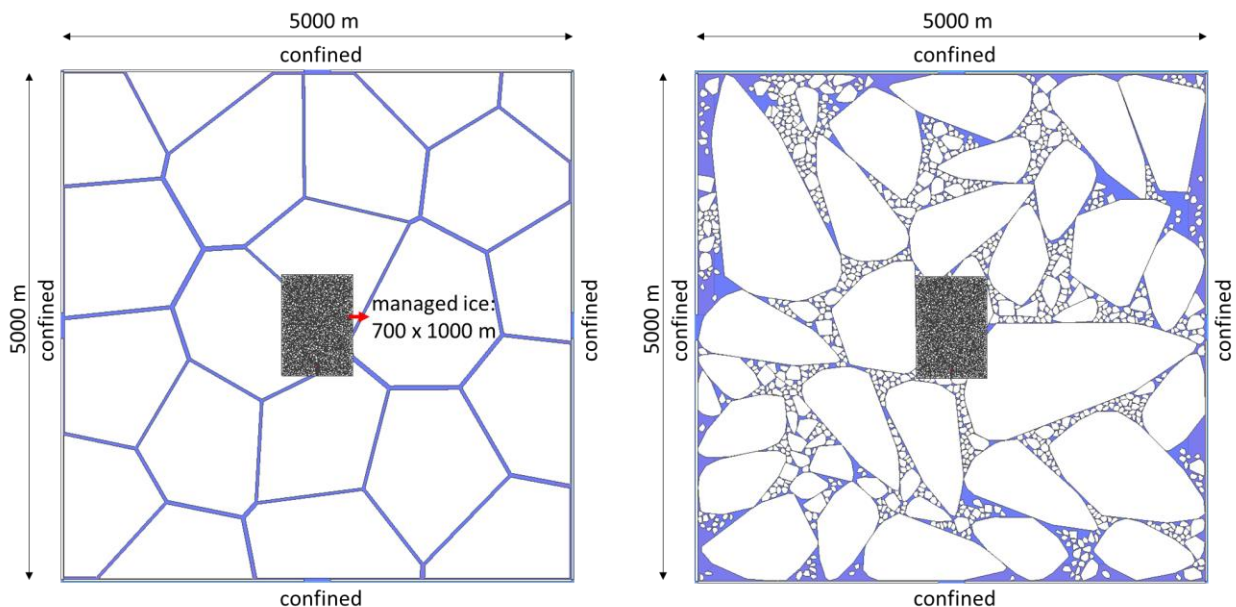


Figure 2. Numerical representation of far-field conditions with difference formation histories. Left: far-field #1. Right: far-field #2.

Figure 3 shows the third simulated boundary condition. Here, the far-field is represented by rigid walls covering 90% of the outer boundary. The managed ice field and initial ship position and orientation in the simulations with far-field conditions #1 and #2 is equal to the managed ice and ship position shown in Figure 3.

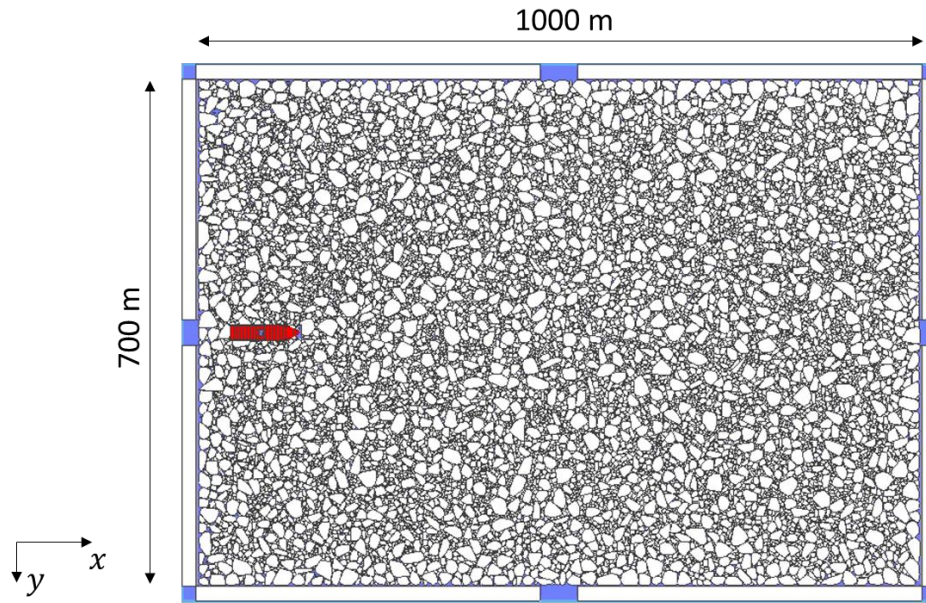


Figure 3. Broken ice field confined for 90% by rigid walls.

### Initial in-plane pressure conditions

For both ship geometries, seven simulations were performed in which in-plane pressure was applied as a one-sided external horizontal pressure  $P$ . The simulation set-up is shown in Figure 4. Three sides are represented by dynamic bodies with masses  $m_1$  (side at  $y = -0.5W$ ) and  $m_2$  (side at  $x = 0$  and  $x = L$ ). This type of confinement is chosen to represent the inertial resistance of the far-field, such that ice acceleration caused by (release of) in-plane pressure is realistically captured. The masses  $m_1$  and  $m_2$  are equivalent in mass to a far-field extending 11 km in the  $-y$  direction and 37 km to both sides in the  $x$ -direction. The value of pressure  $P$  varies from 0 to 6 kN/m in steps of 1 kN, leading to seven different ice pressure conditions.

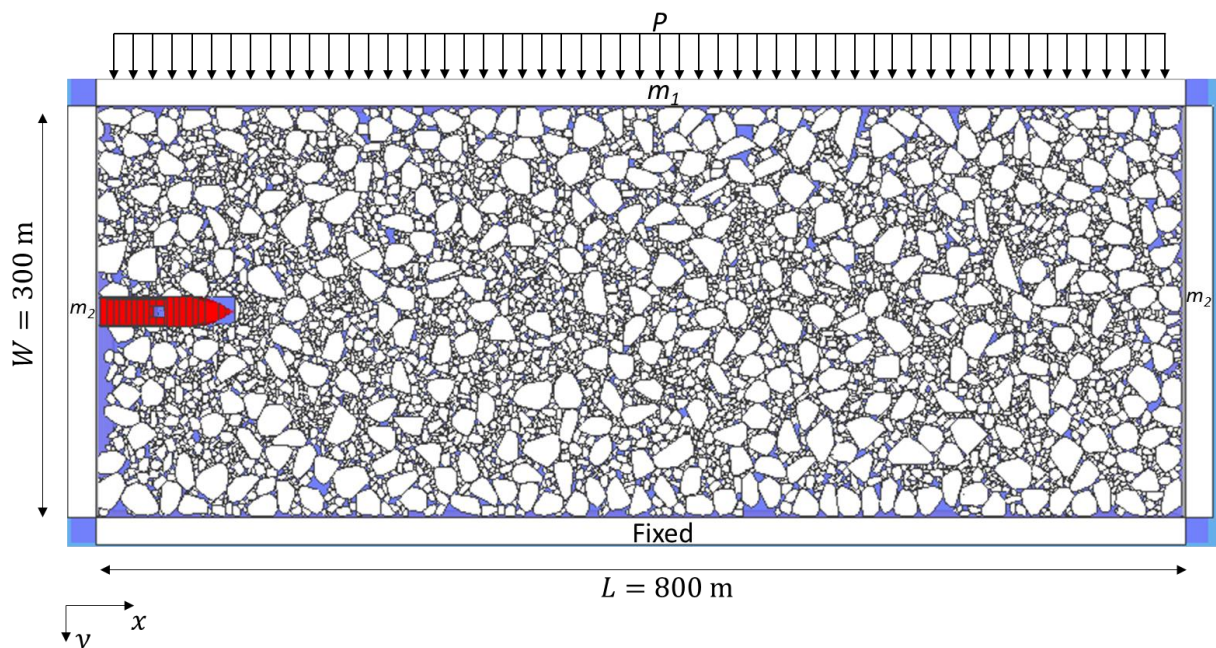


Figure 4. Simulation configuration with constant external pressure field.

## **SIMULATION METHOD**

The numerical simulations were performed with the Simulator for Arctic Marine Structures (SAMS). SAMS is a numerical simulator designed for the modelling of ice-structure and ice-ship interaction. SAMS uses the non-smooth discrete element method. In each time step, contact forces are calculated implicitly by solving a mixed linear complementarity problem. The method allows for relatively large time step sizes, but the resolution of forces within each time step is more demanding than in explicit methods. The method is described in detail in van den Berg et al. (2018). Bending and splitting failure of ice floes is considered using analytical solutions described in (Lu et al., 2018, 2015a, 2015b). Hydrostatic and hydrodynamic forces on ice floes are considered by using drag coefficients and the local velocity of the triangulated ice floe geometries, as described in Tsarau (2015). An overview of the combined model components is given in Lubbad et al. (2018) (This short description of the SAMS model has been used before in van den Berg et al. (2020a)).

## **RESULTS AND INTERPRETATION**

The simulation results show that the boundary conditions and the in-plane pressure both have a strong influence on the ice resistance. The influence of boundary conditions and in-plane pressure is generally higher for the Dina Polaris hull geometry. This is attributed to the higher average normal angle of the bow ( $72^\circ$ , e.g., the hull is closer to vertical). The high normal angle at the bow leads to in-plane ice floe displacement as the predominant clearing mechanism. The Vidar Viking bow has a much lower average normal angle ( $38^\circ$ ) and clears the broken ice mainly by out-of-plane displacement. The resistance caused by in-plane ice clearing is more strongly influenced by boundary conditions and in-plane pressure than out-of-plane ice clearing. The results are discussed in more detail in the following sections.

### **Simulations with no initial in-plane pressure**

In the simulations with no initial in-plane ice pressure, different choices of boundary conditions can lead to significant changes in the mean ice resistance. Figure 5 shows the mean ice resistance of both hull geometries for the three simulated boundary conditions.

A far-field with long open leads (far-field #1) leads to the lowest ice resistance. This far-field condition prevents the occurrence of high in-plane pressures, as the far-field ice floes do not form a continuous contact network (local in-plane pressure may still occur because of the inertial and drag resistance on the ice floes).

Far-field #2 leads to an increase in ice resistance because the displacement of far-field floes is constrained by the continuous contact network. The ice resistance increases more strongly for the Dina Polaris hull geometry. The boundary conditions have a stronger influence on the ice resistance for the Dina Polaris hull geometry because of the higher average normal angle at the waterline. Because of this bow feature, the ice is mainly cleared by in-plane displacement, while the Vidar Viking mainly clears the ice by out-of-plane displacement.

Rigid confining walls lead to the highest ice resistance for both hull geometries. Again, the ice resistance of the Dina Polaris is influenced more strongly by the boundary conditions than the ice resistance of the Vidar Viking.

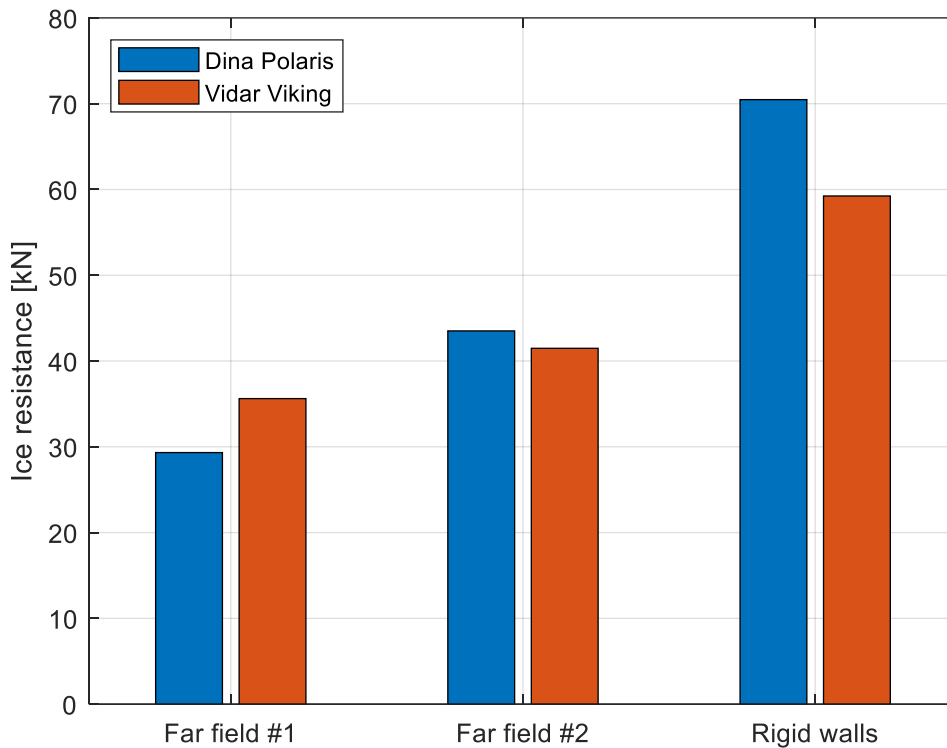


Figure 5. Influence of the boundary conditions on the ice resistance.

### Simulations with in-plane pressure

The simulation results from the simulations with in-plane pressure show a strong increase in the ice resistance for an ice pressure increase from 0 to 6 kN/m. Figure 6 shows the ice resistance as a function of the in-plane pressure for both simulated hull geometries. The ice resistance increases more strongly for the Dina Polaris than for the Vidar Viking. As explained in previous section, this can be attributed to the difference in ice clearing mechanisms.

Figure 7 and Figure 8 show snapshots of ice clearing for both hull geometries at no in-plane pressure and at 6 kN/m in plane pressure, respectively. At no in plane pressure, ice predominantly clears around the Dina Polaris by in-plane displacement. At an in-plane pressure of 6 kN/m, the main ice clearance mechanisms for the Dina Polaris are in-plane displacement, ice splitting failure, ice floe rafting and (occasionally) out-of-plane displacement.

For the Vidar Viking hull geometry, ice is cleared by a mixture in in-plane and out-of-plane displacement at no in-plane pressure. At an in-plane pressure of 6 kN/m, ice is cleared by a mixture of out-of-plane displacement and bending & splitting failure.

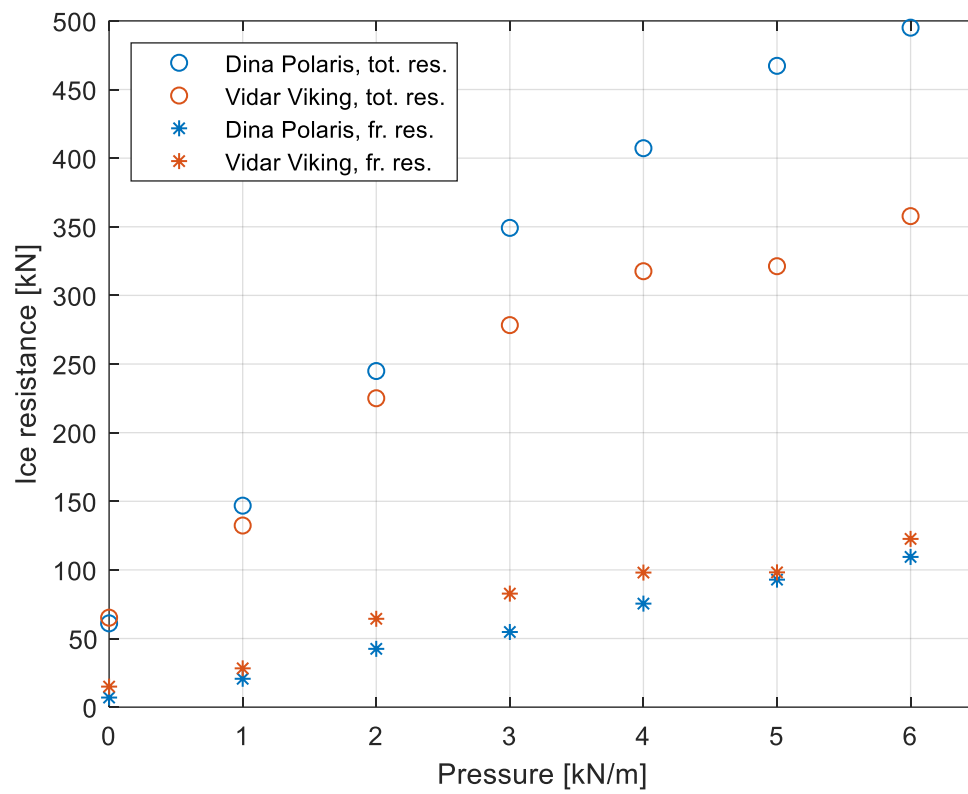


Figure 6. Ice resistance as a function of in-plane pressure.

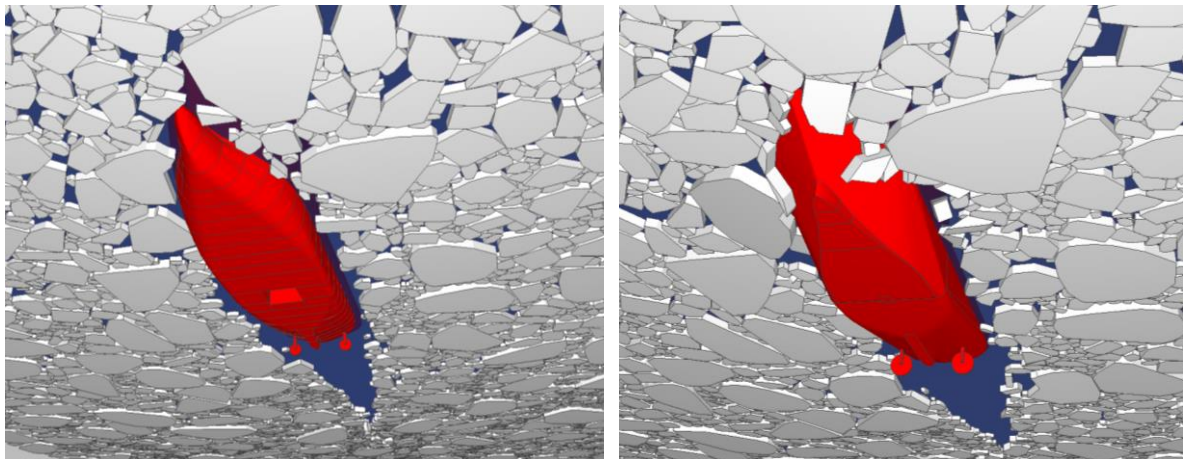


Figure 7. Ice clearance with no in-plane pressure. Left: Dina Polaris. Right: Vidar Viking.

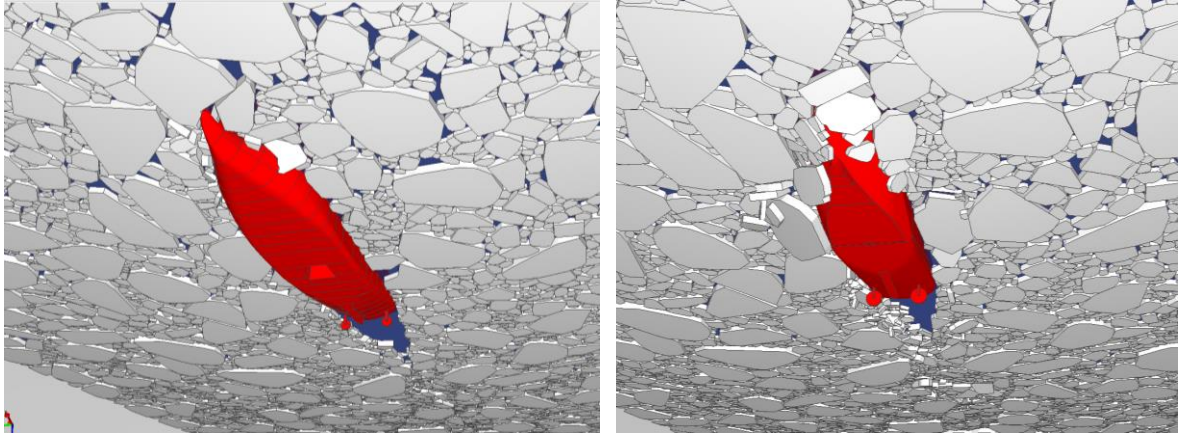


Figure 8. Ice clearance with an in-plane pressure of 6 kN/m. Left: Dina Polaris. Right: Vidar Viking.

Figure 9 shows the relative contribution of frictional resistance to the total resistance as a function of the in-plane ice pressure. The contribution of friction increases with in-plane pressure, and is generally higher for the Vidar Viking. However, for the simulated range of in-plane pressures, the frictional resistance never exceeds 35% of the total resistance. Thus, frictional resistance along the parallel mid-bodies of the ships is not the main mechanism behind the increase in resistance. A simple analytical check shows that the numerically predicted frictional resistance has a reasonable value. Assuming that the broken ice field would exert a uniform pressure equal to the far-field pressure on the ship hull at the waterline over its full waterline length would give frictional resistance values of:

$$F_{fr} = 2 \cdot L_{wl} \cdot P \cdot \mu_{is}$$

where  $L_{wl}$  is the waterline length,  $P$  is the far-field pressure and  $\mu_{is}$  is the ice-structure friction coefficient. This simple approximation would result in frictional resistance values of 116 kN for the Dina Polaris and 90 kN for the Vidar Viking. This is comparable to the simulated frictional resistance values at 6 kN/m ice pressure of 109 kN/m and 122 kN/m, respectively.

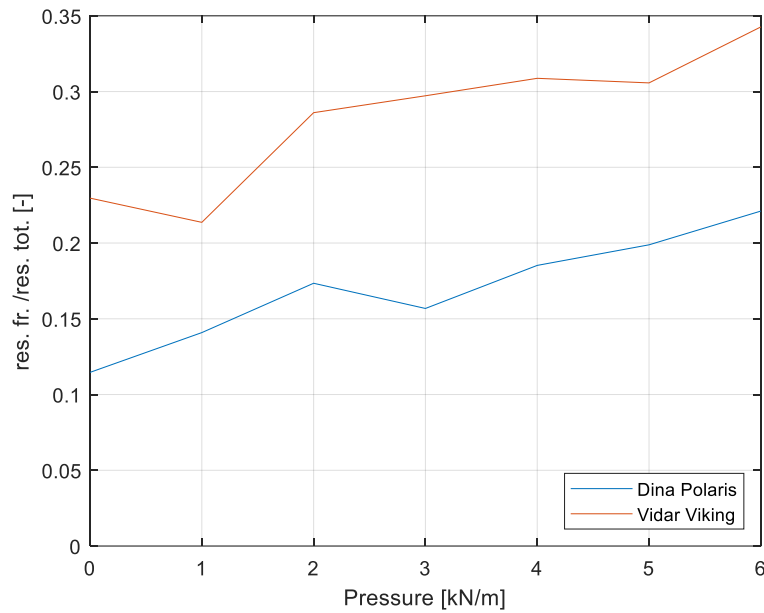


Figure 9. Contribution of frictional resistance to the total ice resistance as a function on in-plane pressure.

## DISCUSSION ON RESULT VALIDITY AND LIMITATIONS

The results presented in this study are based on numerical simulations of ice-ship interaction. As any numerical model, the simulator SAMS is a simplified representation of reality. The following numerical assumptions may influence the results presented in this study:

- All ice floes are represented as planar features with vertical sides. This may lead to higher in-plane pressure as a result of ship movement relative to the ice field than what would occur in reality.
- Frictional forces at ice-ice and ice-structure contacts are approximated by the assumption of coulomb friction. A single friction coefficient of 0.25 (ice-ice) or 0.1 (ice-structure) is assumed. Previous studies (van den Berg et al., 2019) show that the frictional interaction forces have a strong effect on ice floe clearance behaviour.
- Ice floe rafting is implement as described in van den Berg, et al., (2020). This rafting model has not yet been validated against full-scale data. Assumptions on the rafting are expected to have a strong influence on the simulation outcome. The influence of numerical rafting assumptions has not been considered in this study.

Note that other numerical simplifications, such as the numerical representation of ice failure and hydrodynamics, may also influence the results. However, based on the results of previous studies, these factors are expected to be of smaller influence on the result of this study than the assumptions listed above. The validity of the results presented in this study is limited to the sets of parameters that have been simulated:

- Broken ice conditions representing managed ice, with the floe size and thickness distribution as listed in Table 1/ Table 2, with a single set of ice floe shapes.
- A width of the managed ice field of 700 m for the simulations with no initial in-plane pressure and a width of 300 m for the simulations with in-plane pressure.

- External pressure represented as a distributed force on a rigid beam over the full domain length. Different assumptions on the inertial properties of the (virtual) far field ice compared to the simulated in-plane pressure are expected to influence the results.

## CONCLUSIONS

Given the simulation results, and the study limitations as described above, the following conclusions are considered supported by the data:

- For the simulated floe size distribution and ice pressure range, the effect of in-plane ice pressure on the ice resistance is dependent on the hull shape at the waterline. A steeper normal angle at the bow (closer to vertical) leads to a stronger effect of in-plane pressure. The effect of in-plane pressure is stronger because in-plane ice displacement is a more dominant clearing mechanism for steeper normal angles. Ice pressure restricts in-plane clearance.
- In the pressure range simulated in this study, ice friction along the parallel midbody of the ship is not likely to be the governing source of additional ice resistance. Rather, the change in ice clearance behaviour causes the most significant increase in resistance. At no or low in-plane pressure, the ice may clear by in-plane displacement. In-plane pressure and/or confinement inhibits in-plane displacement of ice floes.
- In-plane ice pressure is partly caused by the propagation of the ship in combination with the far-field conditions. In the numerical simulation results, the effect of far-field conditions is significant, even though the broken ice fields up to 350 m on either side of this ships are the same. However, for the simulated floe size distribution and ice pressure range, the effect of ‘external’ ice pressure, caused by wind and current, is much stronger than the in-plane pressure caused by ship propagation.

## ACKNOWLEDGEMENTS

The authors would like to acknowledge the contribution of Åke Rohlén and Ulf Hedman of Arctic Marine Solutions (AMS) for providing the ship hull geometries and ice conditions and the contribution of Shreesha Govinda in digitizing the hull geometries from line drawings.

## REFERENCES

- ArcOP [WWW Document], 2022. URL [www.ecord.org/expedition377/](http://www.ecord.org/expedition377/)
- Copernicus Sentinel 2 satellite data (2016-2019). Retrieved from <https://scihub.copernicus.eu/> on 15-3-2021. Processed by ESA.
- Lemieux, J.F., Bruno Tremblay, L., Plante, M., 2020. Toward a method for downscaling sea ice pressure for navigation purposes. *Cryosphere* 14, 3465–3478.
- Li, F., Kujala, P., Montewka, J., 2019. A ship in compressive ice: an overview and preliminary analysis. *Proc. Int. Conf. Port Ocean Eng. under Arct. Cond. POAC 2019-June*.
- Lu, W., Lubbad, R., Løset, S., 2015a. In-plane fracture of an ice floe: A theoretical study on the splitting failure mode. *Cold Reg. Sci. Technol.* 110, 77–101.
- Lu, W., Lubbad, R., Løset, S., 2015b. Out-of-plane failure of an ice floe: Radial-crack-initiation-controlled fracture. *Cold Reg. Sci. Technol.* 119, 183–203.

- Lu, W., Lubbad, R., Shestov, A., Løset, S., 2018. Parallel channels' fracturing mechanism during ice management operations. Part I: Theory. *Cold Reg. Sci. Technol.*
- Lubbad, R., Løset, S., Lu, W., Tsarau, A., van den Berg, M., 2018. An overview of the Oden Arctic Technology Research Cruise 2015 (OATRC2015) and numerical simulations performed with SAMS driven by data collected during the cruise. *Cold Reg. Sci. Technol.* 156, 1–22.
- Tsarau, A., 2015. Numerical Modelling of the Hydrodynamic Effects of Marine Operations in Broken Ice. Norwegian University of Science and Technology.
- Turnbull, I.D., Bourbonnais, P., Taylor, R.S., 2019. Investigation of two pack ice besetting events on the Umiak I and development of a probabilistic prediction model. *Ocean Eng.* 179, 76–91.
- van den Berg, M., Lubbad, R., Løset, S., 2020a. Statistical Analysis of Results from Ice-Tank Tests with Broken Ice, in: 25th IAHR International Symposium on Ice. Trondheim.
- van den Berg, M., Lubbad, R., Løset, S., 2020b. Repeatability of ice-tank tests with broken ice. *Mar. Struct.* 74, 102827.
- van den Berg, M., Lubbad, R., Løset, S., 2019. The effect of ice floe shape on the load experienced by vertical- sided structures interacting with a broken ice field. *Mar. Struct.* 65, 229–248.
- van den Berg, M., Lubbad, R., Løset, S., 2018. An implicit time-stepping scheme and an improved contact model for ice-structure interaction simulations. *Cold Reg. Sci. Technol.* 155, 193–213.